# Design and Fabrication of Low-Loss Hydrogenated Amorphous Silicon Overlay DBR for Glass Waveguide Devices

Jaeyoun Kim, Kim A. Winick, *Senior Member, IEEE*, Catalin Florea, and Michael McCoy

***Abstract*—We report a methodology for the design of low-loss, high-reflectivity, amorphous silicon, overlay DBRs for glass waveguide devices. In order to improve the DBR reflectivity while minimizing the DBR-induced loss, we theoretically determine the optimum overlay thickness and establish an iterative deposition procedure to achieve this value. Details of the design criteria, measurement of the design parameters, and a numerical analysis of the resulting overlay DBR structure are presented. The deposition and characterization methods for low-loss overlay materials are also discussed. We apply the procedures to implement a multiple-wavelength source consisting of an array of overlay DBR waveguide lasers on a single Er/Yb-doped glass substrate. The lasing wavelengths of the laser array are linearly related to the width of the mask openings used to fabricate the waveguides. One laser with an 8.5-mm-long gain section and a 1.5-mm-long overlay DBR had a launched pump power threshold of 29 mW and an 8.5% slope efficiency. Good agreement is observed between theory and measurement results.**

***Index Terms*—Amorphous semiconductors, distributed Bragg reflector (DBR) lasers, erbium, optical waveguides, ytterbium.**

## I. Introduction

With the rapid growth of wavelength-division multiplexed (WDM) networks, the integration of distributed Bragg reflectors (DBRs) with glass waveguides has attracted substantial research interest. Integrated DBRs enable the fabrication of wavelength filters and single/multiple-wavelength lasers in glass waveguides. Glass waveguide DBRs are usually implemented by ion-milling [1], [2] or through direct UV-induced modulation of the glass's refractive index [3], [4]. Ion-milling is the dominant method for corrugating multicomponent glass surfaces, but the method has a few technical drawbacks. The ion-milling process is slower ($\sim$15 nm/min reported in [1]) than other dry etching techniques for semiconductor processing. The process also generates heat that deforms the photoresist mask and consequently limits the etch depth. A more serious problem is the similar etch rate of photoresist and glass that makes the fabrication of deep gratings difficult without the additional deposition of a metal layer on top of the photoresist pattern. Moreover, in the case of a low-index-contrast waveguiding structure, direct surface corrugation requires very deep and/or long gratings to achieve a high reflectivity. The UV grating writing technique, which is widely used in optical fibers, requires that the glass be suitably photosensitive. Photosensitivity, however, is not usually present in multicomponent glass substrates that also have good rare-earth doping and waveguide fabrication properties. Hussell *et al.* proposed a new technique that simplifies DBR fabrication by depositing an overlay of an easy-to-etch material on top of the waveguide [5]. A grating is subsequently etched into the overlay rather than into the waveguide surface itself. With proper choice of the overlay material, the etching can be simpler and faster (e.g., $\sim$ 60 nm/min for amorphous silicon with reactive ion etching). If the refractive index of the overlay is much higher than the effective index of the waveguide mode, then the structure shows an additional advantage of a significantly enhanced interaction between the waveguide mode and the overlay. This enhanced interaction permits the fabrication of short DBRs which have high reflectivities [6]. Furthermore, compared with glass, the overlay may have desirable thermooptic [7] and/or nonlinear optical properties [8] which permit electrical or all-optical control of the DBR structures. The thinness of the overlay should also allow the gratings to be under-coated or conformally over-coated with other electrooptic or thermooptic materials [9]. This type of coating may not be an option for deep ion-milled gratings. Conese *et al.*, however, pointed out that the higher overlay refractive index can also cause an additional loss whose value depends on the overlay thickness [6]. Achieving a high DBR reflectivity, while limiting the loss, requires careful control of the overlay thickness and its complex refractive index. To date, only two groups have been reported overlay DBRs [5], [10]. Hussell *et al.* demonstrated amorphous silicon overlay DBRs on lithium niobate waveguides, but did no work with glass. Pissadakis *et al.* reported DBRs on ion exchanged glass waveguides fabricated in indium oxide and tantalum oxide overlays, but was only able to achieve modest reflectivities of about 40% with relatively long (25 mm) DBRs. Neither Hussell nor Pissadakis incorporated their gratings into a functional device.

In this work, we present design and fabrication techniques which allow the implementation of low-loss, amorphous silicon, overlay DBRs on glass suitable for device applications. We reduce the loss in two ways: first, by careful selection of the overlay deposition technique, and secondly, by tailoring the overlay/waveguide mode profile through proper selection of the

Manuscript received September 3, 2002; revised September 26, 2002.

J. Kim and K. A. Winick are with the Department of Electrical Engineering and Computer Science, University of Michigan, Ann Arbor, MI 48109 USA.

C. Florea is with the Applied Physics Program, University of Michigan, Ann Arbor, MI 48109 USA.

M. McCoy is with the Northstar Photonics, Inc., Maple Grove, MN 55369 USA.

Digital Object Identifier 10.1109/JSTQE.2002.806720

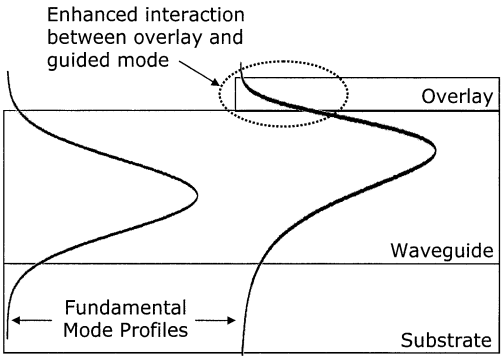


Fig. 1. Schematic diagram of overlay/waveguide structure showing the enhanced interaction between the overlay and the guided mode. The enhancement can improve the DBR reflectivity after the patterning a grating on the overlay.

overlay thickness. For the latter, we utilized previous reports that studied how propagation loss is related to the overlay-induced changes of the mode profile and the overlay characteristics [6], [11]. Based on these results, we devised an approach to achieve an appropriate overlay structure that consists of the following four steps: characterization of the waveguide, measurement of the complex refractive index of the overlay material, mode analysis of the combined overlay/waveguide structure, and control of overlay thickness. To illustrate this approach, we have implemented low-loss overlay DBRs and an array of multiple-wavelength Er/Yb overlay DBR glass waveguide lasers. We will present the overlay design procedure in Section II of this paper, DBR fabrication details in Section III, and active and passive device performance in Section IV.

## II. Overlay DBR Design Issues

### A. Modal Study of Overlay/Waveguide Structure

Fig. 1 shows a sketch of the overlay/waveguide structure. The waveguide underneath the overlay may have a refractive index profile that is either step-index or graded. The overlay material is usually selected so that its refractive index is much higher than the effective index of the unperturbed (i.e., without overlay) waveguide mode. This selection enhances interaction between the mode and the overlay. By choosing the proper overlay thickness and complex refractive index, it is possible to control the propagation characteristics of the waveguide mode as a function of wavelength or polarization state. This concept of overlay/waveguide structures for mode control evolved from the theory of metal-clad waveguide polarizers [12]. The use of semiconductor and dielectric claddings was proposed for low-loss operations in an optical regime [13], [14]. Comprehensive theoretical studies of overlay/waveguide structures also led to a better understanding of their mode characteristics [6], [11]. The overlay/waveguide structure has been utilized for glass waveguide applications, including filtering [15], polarization discrimination [16], and detectors [17]. The overlay DBRs integrated with waveguides are especially relevant to the work reported here [5], [10]. A closely related structure that utilizes the same concept is the side-polished fiber device where an overlay is employed to enhance the evanescent coupling of the field for filtering and sensing applications [18], [19].

The complex refractive index and the thickness of the overlay are the two most important parameters that control characteristics of the propagation mode of the overlay/waveguide structure. It is important to take the imaginary part of the refractive index into consideration, since the overlay material often exhibits high loss in optical regime. Once the complex refractive index is fixed by the material selection, the overlay thickness becomes the main parameter that controls the mode characteristics (profile and complex effective index) of the overlay/waveguide structure. By making the overlay thicker, one can enhance the interaction between the waveguide mode and the overlay through redistribution of mode power from the waveguide into the overlay. The enhanced interaction results in higher reflectivity when the overlay is corrugated to form a DBR. A tradeoff exists, however, between interaction enhancement and propagation loss. The redistribution of mode power into the overlay may increase the propagation loss if the optical loss of the overlay material is higher than that of the waveguide. On the other hand, if the overlay is too thin, then the interaction becomes weaker and the DBR will exhibit low reflectivity. With the waveguide characteristics and the overlay refractive index determined, the overlay thickness should be chosen to yield a high degree of overlay/waveguide interaction while maintaining an acceptable propagation loss.

The mode characteristics can be highly sensitive to the overlay thickness near the desirable value. A simplified modal analysis of an overlay/waveguide structure clarifies this issue. Fig. 2(a) shows the overlay/waveguide structure approximated by four, planar, step-index layers (substrate, waveguide, overlay, air) and the corresponding material parameters. The complex effective index of the overlay/waveguide was obtained by solving the complex characteristic equation [20]. The reflectivity of the corrugated overlay DBR was estimated by modeling the DBR as a multiple stack of high- and low-index layers, which yields the following expression for the reflectivity $R$ for TE polarization [21]

$$R = \tanh^2\left(\frac{\Delta N_{\text{eff}}}{N_{\text{eff}}} m\right) \tag{1}$$

where $N_{eff}$ is the real part of the effective index of the guided mode without the overlay, $\Delta N_{\text{eff}}$ is the change in the real part of the effective index of the guided mode when the overlay is added, and $m$ is the number of grating periods. Fig. 2(a) and (b) illustrates the mode characteristics as the overlay thickness is varied from 0 to 28 nm. As the overlay thickness is increased from zero, the mode characteristics change gradually. When the overlay thickness reaches 25 nm, the additional propagation loss due to the overlay becomes 0.67 dB/cm and the corresponding reflectivity of a Bragg grating with 5000 periods is 65.13%. With a 3-nm increase in overlay thickness, the additional loss increases to 3.1 dB/cm and the reflectivity becomes 98.19%. For this structure, the desirable overlay thickness lies in the range of 25–28 nm depending on the desired propagation loss and DBR reflectivity. The results clearly indicate that deposition thickness control with nanometer accuracy is required.

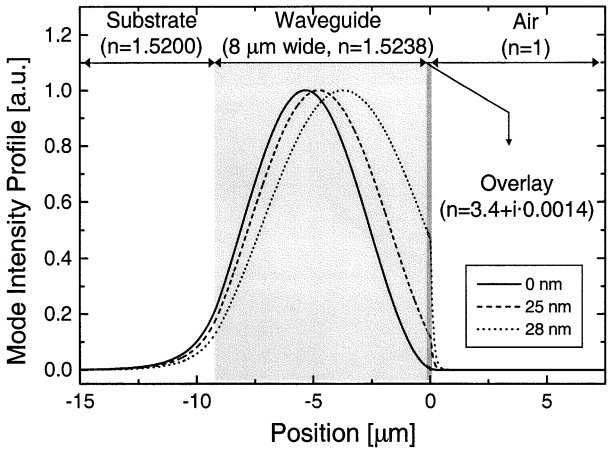


(a)

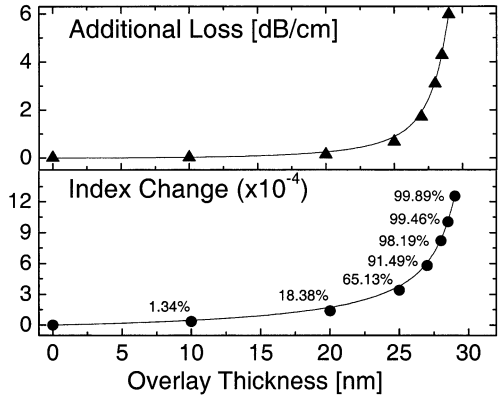


(b)

Fig. 2. (a) Overlay/waveguide structure and the calculated mode profiles. (b) Calculated additional loss, index change, and DBR reflectivity for 5000 periods as a function of overlay thickness.

### *B. Iterative Approach to a Target Thickness*

We have established the following iterative procedure to achieve the target overlay thickness. First, the index profile of the waveguide is obtained by a refractive near-field (RNF) measurement. The complex refractive index of the overlay material is also experimentally determined (details in Section III-A). Next, a finite difference method (FDM) is used to calculate the mode characteristics (i.e., the real and imaginary parts of the effective index and the mode profile) of the overlay/waveguide structure. In order to effectively analyze the structure that simultaneously contains elements measured in nanometers (overlay) and in micrometers (waveguide), we adopt a variable step-size FDM scheme [22]. The full vectorial nature of the computational scheme allows the polarization dependence to be determined. Finally, as a function of overlay thickness, the additional propagation loss is computed from the imaginary part of the effective index and the reflectivity from the real part using (1).

Each iteration cycle consists of a short-duration overlay deposition, followed by a waveguide throughput measurement. The process is terminated when the target overlay thickness is achieved as determined by the throughput loss measurements. In this way, the iterative approach ensures the implementation of a low-loss overlay DBR (detailed application in Section IV-B). Note that an *in situ* monitoring technique [23] or a precisely calibrated deposition system with closed-loop control may eliminate the need for this iterative approach. If the DBR grating has a duty cycle of 50%, then the DBR-induced loss should be half of the overlay-induced loss.

## III. Overlay DBR Fabrication Issues

### *A. Overlay Material and Deposition*

The selection of the overlay material is important since the complex refractive index of the overlay determines the modal and loss characteristics of the overlay/waveguide structure. A good overlay film material must have a high refractive index (compared to the underlying substrate), low loss, and be compact and smooth with low scattering losses. In addition, the deposition and etching of the overlay by conventional semiconductor processing techniques should be easy. We choose amorphous silicon because it meets all of these requirements. It exhibits a high refractive index (2.9–3.4), low inherent loss in the infrared, is easily deposited by sputtering or plasma-enhanced chemical vapor deposition (PECVD), and may be etched using well-developed reactive ion etching (RIE) techniques. We have found that PECVD of amorphous silicon is preferred over sputtering, since the silane gas ($SiH_4$) used in this process results in hydrogenation of the deposited silicon film. The hydrogenation reduces the otherwise high infrared absorption loss of amorphous silicon by passivating the silicon dangling bonds with hydrogen radicals [24]. The hydrogenated amorphous silicon (a-Si:H) also has some desirable thermooptic [7], electrooptic [25], and nonlinear optical properties [8] which may permit electrical or all-optical control of the DBRs.

For our PECVD process, we maintained the chamber pressure at 430 mtorr, the RF plasma power at 90 W (70 $\mathrm{mW/cm^2}$), the silane flow at 100 sccm, and the substrate temperature at 250 °C. We measured the complex refractive index ($n + i\kappa$) of the hydrogenated amorphous silicon (a-Si:H) film using the two-layer interference-fringe measurement technique [26]. For this measurement, an approximately 500-nm-thick layer of a-Si:H was deposited on a 1-mm-thick glass substrate to form a thin etalon of silicon. The spectral transmittance of this etalon was then measured across a 1000-nm range using a spectrophotometer. The transmission data for etalons made with PECVD a-Si:H and sputtered amorphous silicon exhibited typical interference fringe patterns as shown in Fig. 3. The $n+i\kappa$ and the film thickness were estimated by least-square fitting the fringe pattern to the theoretical curve for a two-layer (a-Si:H/glass) etalon. The estimated $n + i\kappa$ of the PECVD a-Si:H layer was found to be $3.40+i0.0014$ at 1530 nm. In comparison, the $n+i\kappa$ of the sputtered, nonhydrogenated amorphous silicon was $2.93+i0.0048$, indicating a loss which is nearly three times larger. Considering the real part of the refractive index, the sputtered silicon film also appears to be less compact. We also note that a recent study has reported that a-Si:H thin films with $\kappa$ values as low as $10^{-6}$ can be achieved provided the PECVD process parameters are optimized [27]. This is a topic for future work.

### *B. Patterning and Pattern Transfer*

For patterning of a photoresist grating on the a-Si:H overlay, we used a Lloyd mirror setup [28]. It was important to measure

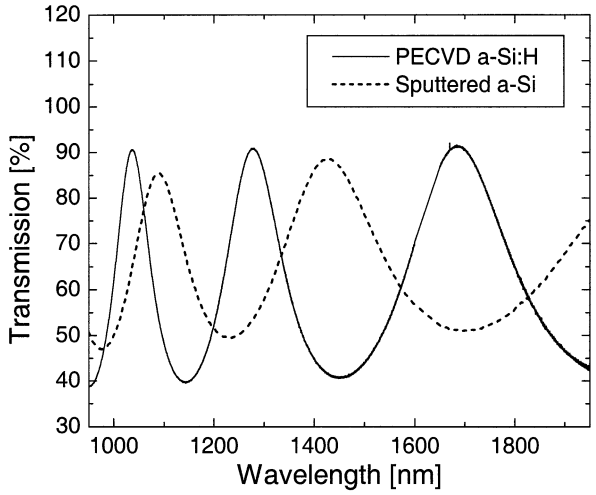


Fig. 3. Interference fringe pattern obtained for transmission through a silicon/glass etalon.

the period of the photoresist grating before permanently transferring the pattern into the overlay by RIE. We measured the grating period by illuminating the photoresist grating with an He–Ne laser beam and measuring the diffraction angle of the first-order backward-diffracted beam. The photoresist grating pattern was then transferred into the overlay by RIE with $CF_4$ as the primary etching gas. RIE is an isotropic etching process that may reduce the duty cycle of the grating as it etches the overlay vertically. Since a reduction in the duty cycle of the grating will result in a lowered DBR reflectivity, we added $CHF_3$ as the secondary processing gas. During the RIE, the radicals from $CHF_3$ form a polymer layer around the a-Si:H surface and consequently induce anisotropy into the etching process. We maintained a $CF_4$ : $CHF_3$ gas flow ratio of 25:28 sccm, a chamber pressure of 50 mtorr, and a 13.56-MHz RF plasma power of 200 W (160 mW/cm$^2$). The flow ratio was chosen based on repeated RIE trials performed at different flow rates followed by inspection of the resulting overlay grating's cross section using a scanning electron microscope (SEM).

### C. Overlay Grating Thickness Measurement

Once fabrication of the overlay DBR was completed, we accurately determined its thickness by measuring the diffraction efficiency of the zeroth-order backward-diffracted beam as a function of incidence angle. The measured values were fitted to the theoretically predicted curves generated using a rigorous coupled-wave analysis (RCWA) [29]. The diffraction efficiency depends on grating depth, period, shape, duty cycle, and the refractive indices of the grating and substrate. The grating depth and duty cycle have the strongest influence on the diffraction efficiency. With the refractive indices and the grating period already determined by techniques described in Sections III-A and III-B, we measured the duty cycle by taking a top-view SEM scan of the grating. Since the grating cross-section usually assumes a trapezoidal shape, due to residual anisotropy in the RIE etch, we used a multiple-layer approximation of RCWA [30]. The application of this method is described in Section IV.

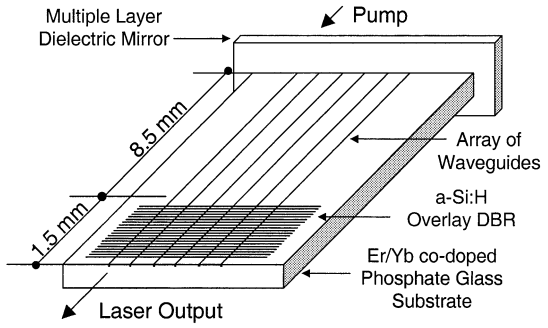


Fig. 4. Schematic diagram of a glass waveguide laser with the overlay DBR.

## IV. Application of the Overlay DBR

Planar waveguide lasers fabricated on rare-earth-doped glass have attracted considerable research interest as lightwave sources for fiber-optic WDM networks. Their advantages include the use of high rare-earth-doping concentrations to achieve compact devices and the potential to integrate a host of optical components on a single substrate. Several glass waveguide DBR lasers [1], [31] and laser arrays [2], [32] have been fabricated with DBRs implemented by ion-milling or UV-induced refractive index modulation. In this section, we demonstrate that low-loss high-reflectivity DBRs can be fabricated in glass waveguides using a-Si:H overlays. We illustrate this technology by applying the design and fabrication techniques of Sections II and III to implement a multiple-wavelength, Er–Yb, overlay-DBR glass waveguide laser array.

### A. Waveguide Modal Analysis

We fabricated the waveguides on an alkali phosphate glass wafer co-doped with $1.0\times10^{20}$ $Er^{3+}$ions/cm$^3$ and $6.0\times10^{20}$ $Yb^{3+}$ions/cm$^3$. Fig. 4 shows a sketch of the overlay/waveguide DBR laser. Six waveguides were formed by $K^+$–$Na^+$ ion exchange through Al mask openings ranging in width from 1.5 to 3.0 $\mu$m. Following the ion exchange, the wafer was diced and its end faces were polished perpendicular to the waveguides. In order to estimate the waveguide propagation loss, we used the Fabry–Pérot fringe measurement technique on identical waveguides fabricated in undoped glass of the same composition [33]. The measurement results of the waveguides fabricated under the same conditions on an undoped wafer showed that the propagation loss is approximately 0.3 dB/cm near 1530 nm. We performed a modal analysis on the waveguide fabricated using a 3-$\mu$m-wide mask opening. The refractive index profile of the glass waveguide (without overlay) was measured using a commercial RNF scanning machine. Fig. 5 shows the two-dimensional (2-D) refractive index profile of the waveguide with a measurement resolution of 0.4 $\mu$m in depth and 0.8 $\mu$m in width. The waveguide has a maximum index change (with respect to the substrate) of $3.8\times10^{-3}$ and exhibits a near-Gaussian refractive index profile that is 8 $\mu$m in depth ($1/e$ point) and 16.8 $\mu$m in width ($1/e$ full width). The FDM grid size for the waveguide portion was the same as the RNF resolution and the vertical grid size for the overlay portion was varied from 0.5 to 1 nm. The FDM

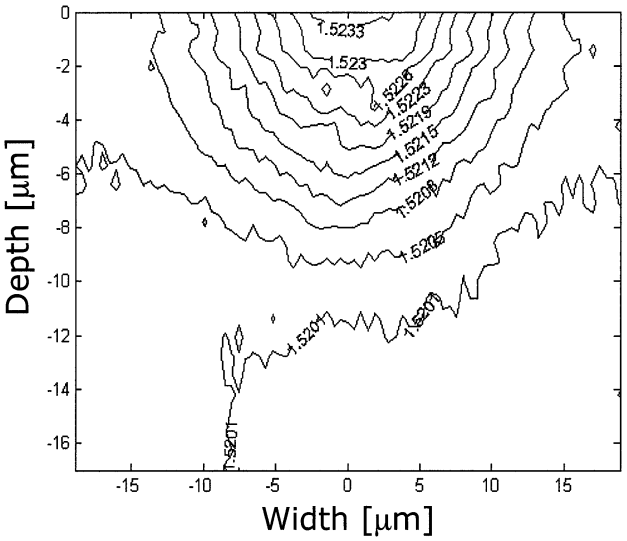


Fig. 5. RNF-scanned refractive index profile of a $K^+$-$Na^+$ ion-exchanged waveguide fabricated through a 3-$\mu$m-wide mask opening.

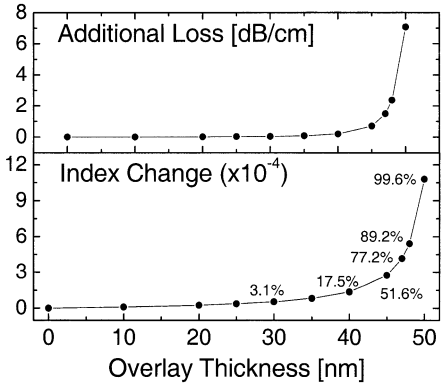


Fig. 6. Additional loss, index change, and DBR reflectivity for 5000 periods as a function of overlay thickness calculated by 2-D fully vectorial FDM. The complex refractive index of a:Si-H and the RNF-scanned index profile of Fig. 5 are utilized for the mode solution.

calculation yields two TE mode-solutions near 1530 nm, with one barely above cutoff. With the same computational grid size in the glass and a grid size of 20 points in the overlay, we obtained the fundamental TE and TM mode solutions as the a-Si:H overlay thickness was varied from 0 to 50 nm. The corresponding propagation loss and change in mode effective index (the real part) of the fundamental TE modes are plotted in Fig. 6. These results are qualitatively similar to those obtained using the simplified four-layer analysis given in Section II-A. Note that both the change in effective index and the propagation loss increase very rapidly when the overlay thickness approaches about 50 nm. Mode profiles for 48- and 50-nm-thick overlays are also shown in Fig. 7 and illustrate the change in mode characteristics as a function of overlay thickness. It is observed that the peak of the mode intensity profile is shifted toward the overlay as the overlay thickness increases. The profiles are also deformed due to the presence of the overlay. As indicated in Fig. 7(d), the modal characteristics of the TM mode are much less affected by the presence of the overlay even though the TE and TM modes were nearly identical in the absence of the overlay. Thus, the overlay DBR is not a high reflector for the TM mode. Based on the above modeling results, we chose a target overlay thickness of 47 nm, corresponding to a 77.2% DBR reflectivity and 1.49 dB/cm additional propagation loss, for a 2.5-mm-long DBR.

### *B. Optimum Thickness Deposition*

With the target thickness determined, we performed the iteration cycle described in Section II. We set the duration of each incremental PECVD to be 2 min. In order to compensate for the changes in free-space/waveguide coupling and variations in the collecting efficiency for each throughput measurement, we excluded one waveguide from deposition by protecting it with metallic cover and measuring the overlay/waveguide throughput relative to this reference waveguide. Fig. 8 shows the changes in measured additional loss due to a 1-cm-long overlay as a function of the total deposition time. The optimum thickness was achieved for a total deposition time between 10–12 min. The measured additional loss after the final deposition was 3 dB/cm indicating that we missed our desired target thickness by approximately 1 nm. We proceeded with the final film that will yield DBR reflectivities of 89.2% and 99.6% for lengths of 0.25 and 0.5 cm (approximately 5000 and 10 000 periods), respectively. The thickness of the overlay was experimentally confirmed after the DBR was fabricated by measuring diffraction efficiency as described in Section III-C. Fig. 9 shows the measurement results superimposed with the RCWA calculations. The inset is the cross-sectional profile of the grating used in this analysis which was obtained from a top-view SEM scan of the structure. The excellent match between the experimental and calculation results confirms that the overlay thickness was in the vicinity of the targeted 48 nm.

### *C. DBR Characteristics*

We patterned a photoresist grating and reactive ion etched the pattern into the 48-nm-thick overlay using the procedures of Section III-B. Fig. 10 is a top-view SEM scan of the a-Si:H overlay DBR seen over the slightly recessed waveguide surface. The grating period was approximately 503 nm. The setup used to measure the spectral response of the overlay DBR consisted of a broad-band amplified spontaneous emission (ASE) source with polarization control and an optical spectrum analyzer (OSA). Light from the polarized ASE source was launched into the overlay DBR waveguide and an OSA scan of the throughput power was collected. Fig. 11 shows the results for a TE-polarized ASE input and a 2.5-mm-long DBR. This device exhibited a 13-dB transmission dip (95% reflectivity) with a 3-dB bandwidth of 0.61 nm. The reflectivity is in good agreement with the calculated results given in Section IV-B of 89.2%. Note that the nonuniform spectral response in the short-wavelength regions which lie immediately outside of the dip is not due to the DBR, but is a result of absorption by the erbium ions in the substrate. A TM-polarized input resulted in less than 2% reflectivity. The large reflection bandwidth is consistent with the high reflectivity and short length of the grating. The length of our high-reflectivity overlay DBR is the shortest reported to date in glass. It is also the first report of an a-Si:H overlay DBR on glass. The determination of the DBR-induced loss by direct measurement of the reflected light

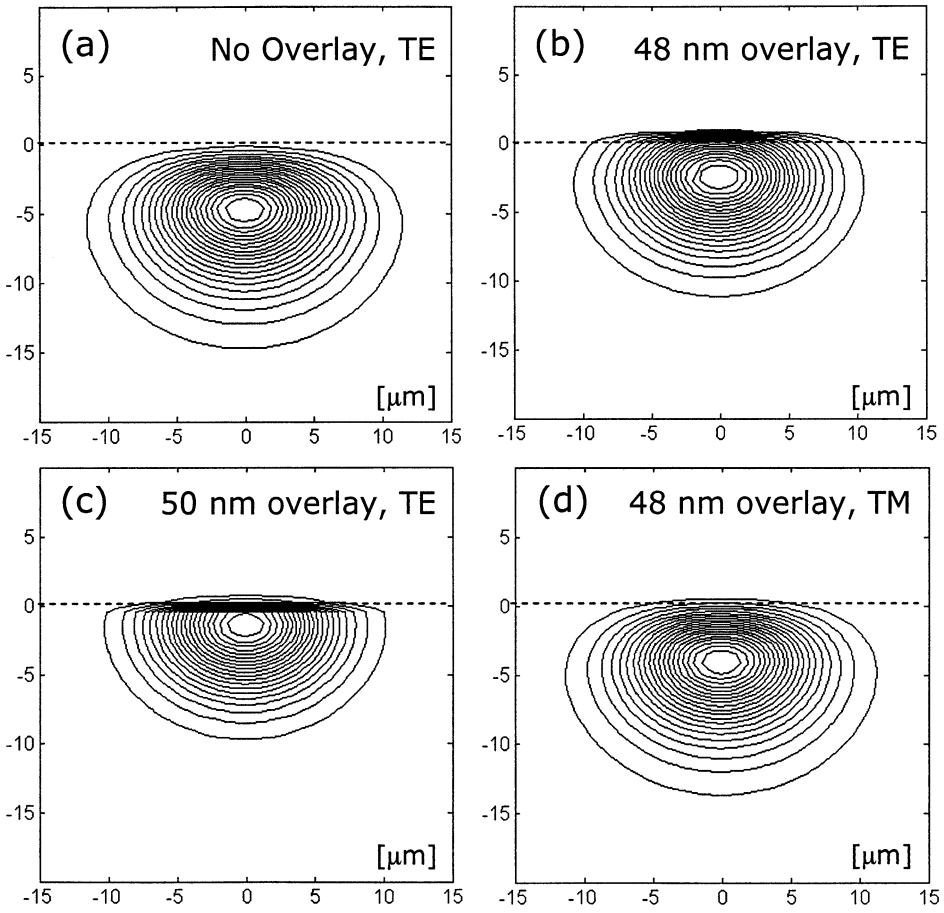


Fig. 7. Two-dimensional mode profiles of the overlay/waveguide structure showing the deformation of the mode as a function of overlay thickness. The degree of deformation parallels that of the index change and additional loss in Fig. 6.

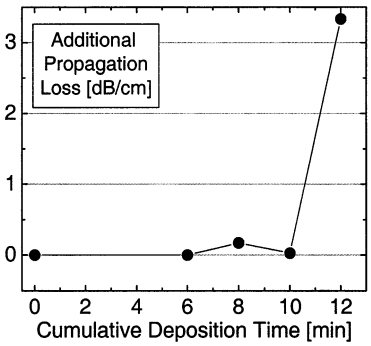


Fig. 8. Measured changes in additional propagation loss due to the a-Si:H overlay as a function of deposition time.

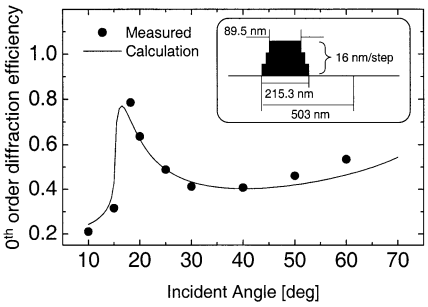


Fig. 9. Measurement of the zeroth-order backward diffraction efficiency for grating depth estimation. The results were fitted to the theoretical prediction of rigorous coupled-wave analysis. The cross-sectional profile and the duty cycle are determined based on the top-view SEM scan.

was unsuccessful due to the difficulties we had in determining other sources of loss in our measurement setup. Throughput measurements, however, indicated that the DBR loss was approximately 2 dB/cm at wavelengths near the transmission dip. Considering the fact that only half of the overlay remains after formation of a grating with a 50% duty cycle, the loss is approximately 0.5 dB/cm higher than theoretically predicted. For our 2.5-mm DBR, the DBR-induced loss is 0.5 dB, which is comparable to the splicing loss between fibers with slightly different core sizes.

### *D. Multiple-Wavelength Laser Array*

As depicted in Fig. 4, the laser array was completed by attaching an external reflector to the waveguide facet on the side opposite to the overlay DBR. The multiple-layer dielectric mirror had a 95% reflectivity near 1530 nm and 86% transmission near 980 nm. Index-matching liquid was used to reduce the Fresnel loss at the waveguide–air–mirror interface. We pumped the overlay DBR waveguide laser with a multimode laser diode that was temperature-tunable near 980 nm. The pump beam was coupled into the waveguide from the external reflector

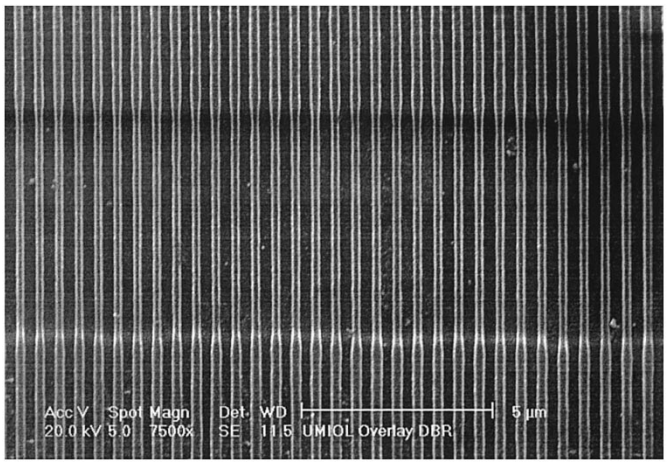


Fig. 10. Top-view SEM scan of an a-Si:H overlay DBR over an ion-exchanged glass waveguide surface. The waveguide surface is slightly recessed due to the mask etching process.

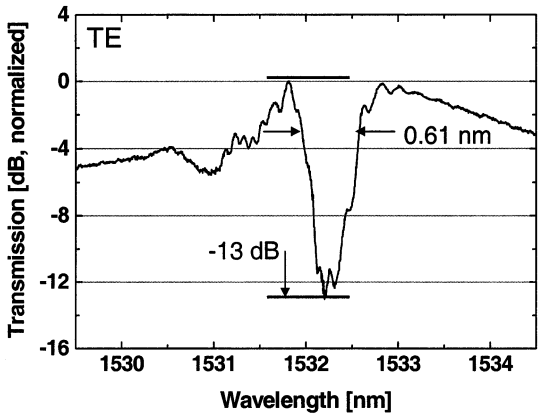


Fig. 11. A 13-dB transmission dip was observed from a 2.5-mm-long a-Si:H overlay DBR. The 3-dB bandwidth is 0.61 nm.

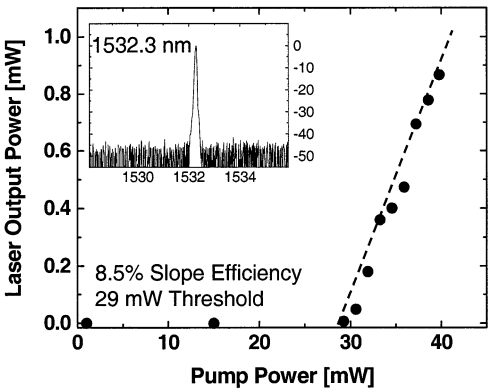


(a)

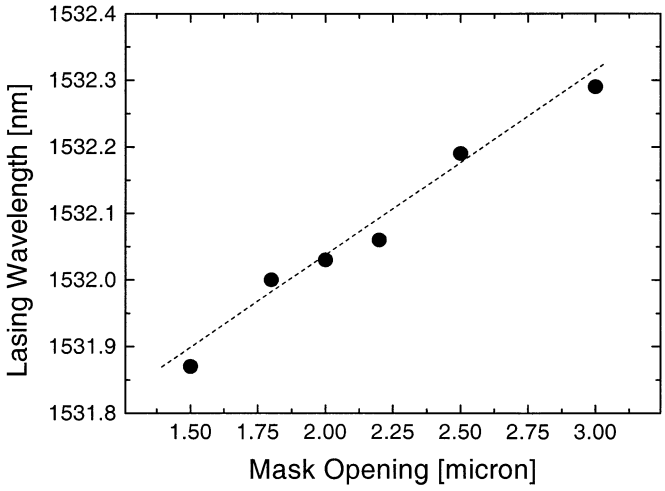


(b)

Fig. 12. (a) The performance of a completed overlay DBR glass waveguide laser. The inset shows the OSA scan of the output spectrum. (b) Multiple-wavelength characteristics of the laser array. The lasing wavelength is in good linear relation with the mask opening for the waveguide fabrication.

side using a 4 × microscope objective lens and the laser output was collected with a 20 × microscope objective lens. We used a multiple layer dielectric filter to block the residual pump beam at the output. In order to accurately determine the laser performance, we measured the launching efficiency of the pump beam using an undoped waveguide sample. We observed lasing from all six a-Si:H overlay DBR lasers. The best lasing performance was obtained from a waveguide formed through a 3-$\mu$m-wide mask opening. The lasing characteristics of this waveguide are presented in Fig. 12(a). This laser had an 8.5-mm-long gain section. We reduce the length of the overlay DBR section from 2.5 to 1.5 mm by RIE in order to increase the slope efficiency of the laser. The reflectivity of the overlay DBR was reduced to about 50% accordingly. The launched pump power threshold was 29 mW and the slope efficiency was 8.5%. The inset of Fig. 12(a) is an OSA scan of laser output with a spectral resolution of 0.07 nm. The laser output was TE polarized. The best performance was obtained when the diode pump wavelength was tuned to 974 nm. In comparison, the 17-mm-long, ion-milled DBR, glass waveguide laser reported by Veasey *et al.* [2] showed a slope efficiency of 26% and a launched pump power threshold power of 50 mW when pumped by a Ti:sapphire laser operating at 974 nm. A 22-mm-long DBR (ion-milled in glass) waveguide laser reported by Callicoatt *et al.* [31] had a 15-mW output power when pumped by two laser diodes with 150 mW of total launched pump power. The glass waveguide DBR laser reported by Madasamy *et al.* was 3.2 cm long, including a 0.5-cm DBR section (ion-milled in glass), and lased with a 13% slope efficiency and a 60-mW launched threshold power when pumped by an unspecified source [32]. Our laser exhibited a low lasing threshold with a shortest DBR thus indicating that a high level of interaction exists between the waveguide and the surface corrugation. The slope efficiency is lower than values reported by others for Er/Yb DBR waveguide lasers but it can be increased at the expense of the lasing threshold which is low in our case. Furthermore, we expect that the slope efficiency can be improved by using a narrow linewidth pump source tuned to the optimum pump wavelength. Due to the limitation in our pump source, we were not able to investigate the laser's performance at high pump powers. We, however, expect that the slope efficiency would not be degraded at these higher pump power levels based on previous reports of a laser with similar characteristics [2]. Fig. 12(b) shows the multiple-wavelength characteristic of the laser array. Note that the lasing wavelengths are linearly related

to the width of the ion-exchange mask opening and the average channel spacing between adjacent wavelengths is on the order of 0.15 nm.

## V. Conclusion

We have demonstrated that short low-loss DBR reflectors can be incorporated into low-index-contrast glass waveguides by using a high refractive index overlay. In order to minimize the loss induced by the overlay and ease fabrication, we selected the overlay material to be a-Si:H deposited by PECVD. PECVD a-Si:H has low inherent infrared absorption because the dangling bonds are passivated with hydrogen. In order to balance the enhanced reflectivity of the overlay DBR with the increased overlay-induced loss, we established an analytic procedure to compute the reflectivity and loss as a function of overlay thickness. Waveguide characterization by 2-D RNF scanning, overlay complex refractive index characterization by the interference-fringe measurements, and modal analysis by fully vectorial 2-D FDM were adopted for these theoretical calculations. Using these results, a target value for the overlay thickness was chosen and an iterative procedure, based on propagation loss measurements, was instituted to deposit films of the appropriate target thickness. A 2.5-mm-long overlay DBR was fabricated which exhibited a 13-dB transmission dip (95% reflectivity) with a 3-dB bandwidth of 0.61 nm. The procedure was also successfully applied to fabricate a multiple-wavelength array of seven Er/Yb overlay DBR lasers. Each laser contained a gain section of length 8.5 mm and an overlay DBR section of length 1.5 mm. Lasing was observed from all seven of the waveguide lasers with an average wavelength channel spacing of 0.15 nm. The lasing wavelength was linearly related to the width of the mask-opening used for waveguide formation. The best laser among the seven had a launched pump power threshold of 29 mW and a slope efficiency of 8.5%. In the future, the thermooptic and nonlinear properties of a-Si:H may be used to demonstrate electrical and all-optical control of overlay DBR.

## References


[1] J. E. Roman and K. A. Winick, "Neodymium-doped glass channel waveguide laser containing integrated distributed Bragg reflector," *Appl. Phys. Lett.*, vol. 61, no. 23, pp. 2744–2746, 1992.

[2] D. L. Veasey, D. S. Funk, N. A. Sanford, and J. S. Hayden, "Arrays of distributed-Bragg-reflector waveguide lasers at 1536 nm in Yb/Er codoped phosphate glass," *Appl. Phys. Lett.*, vol. 74, no. 6, pp. 789–791, 1999.

[3] T. Kitagawa, F. Bilodeau, B. Malo, S. Theriault, J. Albert, D. C. Jihnson, K. O. Hill, K. Hattori, and Y. Hibino, "Single-frequency $Er^{3+}$-doped silica-based planar waveguide laser with integrated photo-imprinted Bragg reflectors," *Electron. Lett.*, vol. 30, no. 16, pp. 1311–1312, 1994.

[4] S. Guldberg-Kjaer, J. Hubner, M. Kristensen, C. Laurent-Lund, M. R. Poulsen, and M. W. Sckerl, "Planar waveguide laser in Er/Al-doped germanosilicate," *Electron. Lett.*, vol. 35, no. 4, pp. 302–303, 1999.

[5] C. P. Hussell and R. V. Ramaswamy, "High-index overlay for high reflectance DBR gratings in $LiNbO_3$ channel waveguides," *IEEE Photon. Technol. Lett.*, vol. 9, pp. 636–638, May 1997.

[6] T. Conese, R. Tavlykaev, C. P. Hussell, and R. V. Ramaswamy, "Finite element analysis of $LiNbO_3$ waveguides with Si or $Si/SiO_2$ overlay," *J. Lightwave Technol.*, vol. 16, pp. 1113–1122, June 1998.

[7] G. Cocorullo, F. G. Della Corte, R. De Rosa, I. Rendina, A. Rubino, and E. Terzini, "Amorphous silicon-based guided-wave passive and active devices for silicon integrated optoelectronics," *IEEE J. Select Topic Quantum Electron.*, vol. 4, no. 6, pp. 997–1002, 1998.

[8] R. M. Ribeiro, L. R. Kawase, W. Margulis, B. Lesche, B. Sahlgren, R. Stubbe, and K. Kleveby, "All-optical control of Bragg grating in semiconductor-coated D-shaped fiber," *Opt. Lett.*, vol. 24, no. 7, pp. 454–456, 1999.

[9] S. Pissadakis, M. N. Zervas, D. A. Sager, and J. S. Wilkinson, "Superstrate index control of waveguide grating reflectivity," *Opt. Lett.*, vol. 27, no. 5, pp. 327–329, 2002.

[10] S. Pissadakis, L. Reekie, M. N. Zervas, J. S. Wilkinson, and G. Kiriakidis, "Gratings in indium oxide film overlayers on ion-exchanged waveguides by excimer laser micromachining," *Appl. Phys. Lett.*, vol. 78, pp. 694–696, 2001.

[11] R. F. Carson and T. E. Batchman, "Multimode phenomena in semiconductor-clad dielectric optical waveguide structures," *Appl. Opt.*, vol. 29, no. 18, pp. 2769–2780, 1990.

[12] K. H. Rollke and W. Sohler, "Metal-clad waveguide as cutoff polarizer for integrated-optics," *IEEE J. Quantum. Electron.*, vol. QE-13, pp. 141–145, Apr. 1977.

[13] T. E. Batchman and J. R. Peeler, "GaAs clad optical-waveguides," *IEEE J. Quantum. Electron.*, vol. QE-14, pp. 327–329, May 1978.

[14] T. E. Batchman and G. M. McWright, "Mode-coupling between dielectric and semiconductor planar waveguides," *IEEE J. Quantum. Electron.*, vol. QE-18, pp. 782–788, Apr. 1982.

[15] I. S. Mauchline and G. Stewart, "Glass integrated-optic channel-dropping filters," *Opt. Lett.*, vol. 18, no. 21, pp. 1801–1803, 1993.

[16] D. L. Veasey, R. K. Hickernell, D. R. Larson, and T. E. Batchman, "Waveguide polarizers with hydrogenated amorphous silicon claddings," *Opt. Lett.*, vol. 16, no. 10, pp. 717–719, 1991.

[17] D. L. Veasey and D. R. Larson, "Integrated optical polarization-discriminating receiver in glass," *J. Lightwave Technol.*, vol. 13, pp. 2244–2249, Nov. 1995.

[18] W. V. Sorin, P. Xorabedian, and S. A. Newton, "Tunable single-mode fiber reflective grating filter," *J. Lightwave Technol.*, vol. 5, pp. 1199–1202, Sept. 1987.

[19] A. Alvarez-Herrero, H. Guerrero, T. Belenguer, and D. Levy, "High-sensitivity temperature sensor based on overlay on side-polished fibers," *IEEE Photon Technol. Lett.*, vol. 12, pp. 1043–1046, Aug. 2000.

[20] K. Schlereth and M. Tacke, "The complex propagation constant of multilayer waveguides: An algorithm for a personal computer," *IEEE J. Quantum. Electron.*, vol. 26, pp. 627–630, Apr. 1990.

[21] K. A. Winick, "Effective index method and coupled-mode theory for almost periodic waveguide gratings-a comparison," *Appl. Opt.*, vol. 31, no. 6, pp. 757–764, 1992.

[22] P. Lusse, P. Stuwe, J. Schule, and H. G. Unger, "Analysis of vectorial mode fields in optical wave-guides by a new finite-difference method," *J. Lightwave Technol.*, vol. 12, pp. 487–494, Mar. 1994.

[23] D. L. Veasey, D. R. Larson, and T. E. Batchman, "In-situ optimization of coupling between semiconductor claddings and dielectric waveguides," *J. Appl. Phys.*, vol. 68, no. 7, pp. 3753–3755, 1990.

[24] R. A. Street, *Hydrogenated Amorphous Silicon.* Cambridge, U.K.: Cambridge Univ. Press, 1991.

[25] M. Zelikson, J. Salzman, K. Weiser, and J. Kanicki, "Enhanced electro-optic effect in amorphous hydrogenated silicon based waveguides," *Appl. Phys. Lett.*, vol. 61, no. 14, pp. 1664–1666, 1992.

[26] L. Vriens and W. Rippens, "Optical constants of absorbing thin solid films on a substrate," *Appl. Opt.*, vol. 22, no. 24, pp. 4105–4110, 1983.

[27] G. Cocorullo, F. G. Della Corte, I. Rendina, C. Minarini, A. Rubino, and E. Terzini, "Amorphous silicon waveguides and light modulators for integrated photonics realized by low-temperature plasma-enhanced chemical-vapor deposition," *Opt. Lett.*, vol. 21, no. 24, pp. 2002–2004, 1996.

[28] R. Kashyap, *Fiber Bragg Gratings*. San Diego, CA: Academic, 1999, pp. 74–77.

[29] M. G. Moharam, D. A. Pommet, E. B. Grann, and T. K. Gaylord, "Formulation for stable and efficient implementation of the rigorous coupled-wave analysis of binary gratings," *J. Opt. Soc. Amer. A*, vol. 12, no. 5, pp. 1068–1076, 1995.

[30] ——, "Stable implementation of the rigorous coupled-wave analysis for surface-relief gratings: Enhanced transmittance matrix approach," *J. Opt. Soc. Amer. A*, vol. 12, no. 5, pp. 1077–1086, 1995.

[31] B. E. Callicoatt, J. B. Schlager, K. L. Silverman, R. K. Hickernell, R. P. Mirin, N. A. Sanford, J. S. Hayden, S. Conzone, and R. Simpson, "Single-frequency and mode-locked Er/Yb co-doped waveguide lasers," in *Proc. LEOS Annual Meeting*, San Diego, CA, 2001, WW1, pp. 576–577.

[32] P. Madasamy, G. N. Conti, P. Poyhonen, Y. Hu, M. M. Morrell, D. F. Geraghty, S. Honkanen, and N. Peyghambarian, "Waveguide distributed Bragg reflector laser arrays in erbium doped glass made by dry Ag film ion exchange," *Opt. Eng.*, vol. 41, no. 5, pp. 1084–1086, 2002.

[33] R. Regener and W. Sohler, "Loss in low-finesse Ti-$LiNbO_3$ optical wave-guide resonators," *Appl. Phys. B*, vol. B36, pp. 143–147, 1985.

**Jaeyoun Kim** received the B.S. degree from Kwangwoon University, Seoul, Korea in 1992 and the M.S. degree from the University of Arizona, Tucson, in 1994, both in electrical engineering.

From 1995 to 1997, he was with the Institute for Advanced Engineering in Seoul, Korea, as a Research Engineer. At the Institute, he was involved in research and development of laser/fiber-optic gyroscopes. In 1997, he started his Ph.D. program in Electrical Engineering in the University of Michigan as an EECS Department Fellow. Currently he is a Research Assistant in Integrated Optics Laboratory. His research interests include linear and nonlinear aspects of fiber optics, design, simulation, fabrication of grating-assisted integrated-optic devices, and their combined utilizations for future optical transmission systems.

**Kim A. Winick** (S'77–M'80–SM'98) was born in New York City, NY, on July 27, 1954. He received the B.S. degree from the Pennsylvania State University, State College, in 1976 and the M.S. and Ph.D. degrees from the University of Michigan, Ann Arbor, in 1977 and 1981, respectively, all in electrical engineering.

From 1981 to 1988, he was a Member of the Technical Staff at the Massachusetts Institute of Technology Lincoln Laboratory, Cambridge, working on millimeter-wave and optical communication systems. In 1988, he joined the faculty of the Department of Electrical Engineering and Computer Science at the University of Michigan where he is currently an Associate Professor. His research interests are in the areas of glass and crystal integrated optics, ultrafast laser micromachining, and information theory and communications.

Dr. Winick is a member of the Optical Society of America.

**Catalin Florea** received the B.S. degree in physics from Bucharest University, Romania, in 1995 and the M.S. degree in electrical engineering and the Ph.D. degree in applied physics from The University of Michigan, Ann Arbor, in 1998 and 2002, respectively. For his Ph.D. work, he worked on glass and lithium niobate ion- and proton-exchanged waveguide devices, as well as on femtosecond direct-write in glass, and PPLN-based techniques in lithium niobate.

His current research interests are fiber-based ultrafast lasers and PPLN-based frequency conversion in ultrafast laser systems.

**Michael McCoy**, photograph and biography not available at the time of publication.